RAPID COMMUNICATIONS

PHYSICAL REVIEW B VOLUME 52, NUMBER 8 15 AUGUST 1995-II

Layer-depopulation- and magnetic-field-induced resistance oscillations in a triple-layer electron system

T. S. Lay, X. Ying, and M. Shayegan
Department of Electrical Engineering, Princeton University, Princeton, New Jersey 08544
(Received 12 April 1995)

The resistance R of a coupled, triple-layer electron system exhibits two distinct types of oscillations as a function of front-gate bias V_{FG} or in-plane magnetic field $B_{\|}$. We observe up to three oscillations in R as a function of $B_{\|}$; these correspond to the passage of the Fermi level through the partial energy gaps arising from the level anticrossings at the intersections of the dispersion curves of the three electron layers. By fixing $B_{\|}$ and decreasing V_{FG}, we observe additional oscillations in R as the system makes triple-to-double and double-to-single layer transitions.

Coupled bilayer electron systems subjected to a perpendicular or parallel magnetic field ($B_{\perp}$ or $B_{\|}$) exhibit intriguing physical phenomena arising from the Coulomb interaction and tunneling. Examples include a unique *even-denominator* fractional quantum Hall effect at filling factor $\nu=\frac{1}{2}$ in a $B_{\perp}$,[1,2] and a new resistance oscillation in a $B_{\|}$ as the Fermi level (E_F) passes through a partial energy gap induced by an anticrossing of the layer energy dispersion curves.[3,4] *Triple*-layer electron systems (TLES's) possessing interlayer and intralayer interactions are also expected to display rich transport properties.[5] The fabrication of high-quality TLES's is particularly challenging, however, and very little experimental work has been reported.[6]

Here we report magnetotransport measurements on a low-disorder TLES in the presence of $B_{\|}$. Using a front-gate bias (V_{FG}) to change the layer densities, we measure the in-plane resistance (R) of the sample as a function of either V_{FG} (at fixed $B_{\|}$) or $B_{\|}$ (at fixed V_{FG}). At a fixed $B_{\|}$, R increases with decreasing V_{FG} as the density decreases but exhibits pronounced oscillations when the TLES undergoes transitions from a triple- to a double- and finally to a single-layer system. In a narrow range of intermediate $B_{\|}$ near 3 T, we observe two additional oscillations in R as a function of V_{FG}, one in the triple-layer regime and the other in the double-layer regime. We show that these oscillations come from the passage of E_F through the energy gaps that are induced by the anticrossing of adjacent layer dispersion curves. In our measurement of R vs $B_{\|}$ at fixed V_{FG}, we observe up to three oscillations; these can also be understood in terms of E_F passing through the level anticrossing gaps. The data, however, show an anomalous behavior: instead of montonically decreasing with decreasing V_{FG} as observed in bilayer systems,[3] the position in $B_{\|}$ of R oscillation from the anticrossing of the central- and bottom-layer dispersions moves to *higher* $B_{\|}$ and reaches a maximum in $B_{\|}$ near the triple-to-double layer transition before finally decreasing. We quantitatively explain all the observations, including this anomalous feature whose origin is an exchange-induced charge transfer from the top to central layer as the top layer is depleted, based on the parameters of our TLES.

The sample is grown by molecular-beam epitaxy and consists of three GaAs quantum wells that are separated by AlAs barriers. The layer thicknesses are 190 Å for the central well, 160 Å for each side well, and 11.3 Å (4 ML) for the AlAs barriers. The structure is confined by undoped (spacer) and Si-doped layers of $Al_{0.35}Ga_{0.65}As$. The thickness of the spacer layer is 1450 Å on the substrate (back) side and 1275 Å on the surface (front) side, and the doping on each side consists of five 1.1×10^{11} cm^{-2} Si planar-doped layers separated by 35 Å of undoped $Al_{0.35}Ga_{0.65}As$. The sample has a van der Pauw configuration with In contacts to the TLES and an Al front gate. All the data were taken in a ^{3}He cryostat ($T\approx0.5$ K). The sample was characterized in a $B_{\perp}$ via measurements of the Hall resistance and Shubnikov–de Haas oscillations. For $V_{FG}=0$ V, the mobility of the sample is 7×10^5 cm^2/V s and the total electron density is 1.42×10^{11} cm^{-2}. We then remounted the sample parallel to the magnetic field.

We first measured the capacitance C of the sample as a function of V_{FG}. Figure 1(a) shows the steplike C-V_{FG} data at $B_{\|}=0$ T. The capacitance drops observed with decreasing V_{FG} result from the depopulation of the layers that increases the distance from the front gate to the nearest electron layer. The TLES makes a triple-to-double layer transition near $V_{FG}=-0.35$ V and a double-to-single layer transition near $V_{FG}=-0.60$ V. These layer-depopulation V_{FG} values are consistent with the results of our subband density measurements, presented later in the paper.

Next, we measured R in a four-point geometry by passing a current $I=0.1$ μA in the y direction and measuring the voltage drop along the same direction. The in-plane magnetic field $B_{\|}$ was applied in the x direction. Figure 1(b) shows R vs V_{FG} at several $B_{\|}$. For all $B_{\|}$, R increases with decreasing V_{FG} as the TLES is depleted of electrons. We observe strong maxima and minima in R, near the same V_{FG} where C-V_{FG} data shows steps. These R oscillations are associated with the depopulations of the top and central layers and are present at all values of $B_{\|}$. A similar oscillation has been observed at $B_{\|}=0$ in double-layer systems with appropriate coupling and has been attributed to the enhanced interlayer Coulomb scattering before the top layer is depleted.[7,8] In addition to these oscillations, at $B_{\|}=2.8$ and 3 T we observe two additional oscillations in R, one in the triple-layer regime ($V_{FG}>-0.35$ V) and the other in the double-layer re-

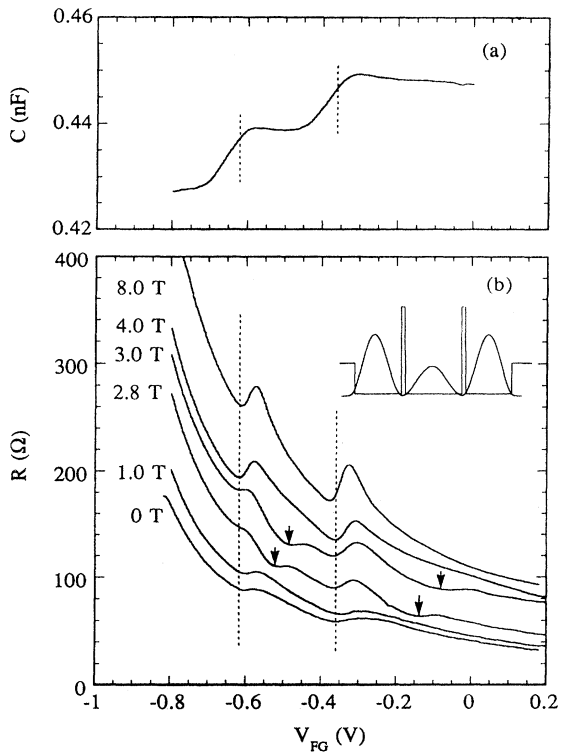

FIG. 1. (a) Capacitance-voltage (C-V_{FG}) data showing the depopulation of the TLES layers. (b) The resistance R vs V_{FG} data at different in-plane magnetic fields showing oscillations in R near the same V_{FG} where the layer depopulation occurs. We have marked the positions of R minima by dotted lines. In an intermediate field range near 3 T, two additional minima (marked by arrows) are observed; these correspond to the level anticrossings. The R scale is for the 0 and 1.0 T data. The 2.8-T data are shifted up by 10 Ω and the higher field traces by 40 Ω for clarity. The inset shows the potential profile of the TLES and the charge distribution at $V_{FG}=0.03$ V when the top and bottom layers have equal densities.

gime ($-0.60<V_{FG}<-0.35$ V), marked by arrows in Fig. 1(b). These oscillations correspond to the $B_{\|}$-induced level anticrossings and are observed in the intermediate field range $2.0<B_{\|}<3.5$ T.

In Fig. 2 we present R vs $B_{\|}$ data measured at several fixed V_{FG}. At $V_{FG}=0$ V, the R vs $B_{\|}$ traces show two resistance oscillations, one near $B_{\|}=1.9$ T and a much stronger one near $B_{\|}=3.6$ T. At a lower $V_{FG}=-0.2$ V, the position of the high-field oscillation at $B_{\|}\approx 3.6$ T essentially remains unchanged but the low-field one moves to a lower $B_{\|}\approx 1.6$ T and a new oscillation appears near $B_{\|}=2.8$ T. When the system is in the double-layer regime ($V_{FG}=-0.40$ or -0.50 V), we observe only one oscillation. Finally, the oscillation completely disappears at $V_{FG}=-0.65$ V where the system is a single layer.

To provide an analysis of the data, we first briefly review the explanation given in Refs. 3 and 4 for the resistance oscillation observed as a function of $B_{\|}$ in *bilayer* electron systems. In a bilayer system at $B_{\|}=0$, the energy vs in-plane wave vector (E-k) dispersions for the electron layers can be represented by two parabolas centered at the origin. Application of a $B_{\|}$ in the x direction displaces the crystal momenta

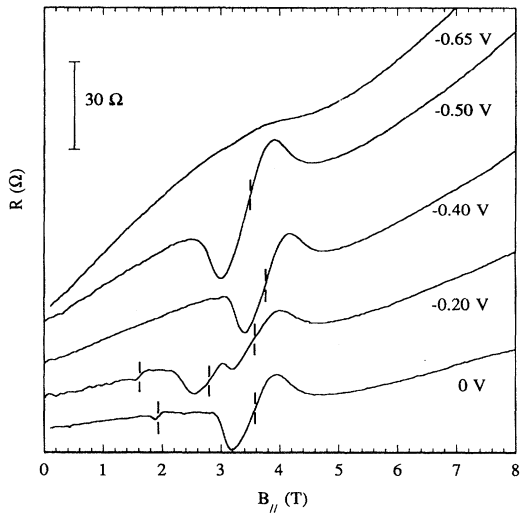

FIG. 2. R vs $B_{\|}$ data at different V_{FG}. Here we observe up to three oscillations in R for the triple-layer system ($V_{FG}>-0.3$ V) and only one oscillation when the system becomes double layer ($-0.6<V_{FG}<-0.3$ V). No oscillations are observed for the single-layer system ($V_{FG}=-0.65$ V). The traces are shifted vertically for clarity and the dashed signs mark the B_{mean} of the oscillations.

k_y of the two layers, and therefore their dispersion parabolas, by an amount $\Delta k_y=d/l^2$, where d is the interlayer distance and $l=(\hbar/eB_{\|})^{1/2}$ is the magnetic length. If the two layers are coupled, a level anticrossing takes place at the interaction of the dispersion parabolas leading to a partial energy gap (for electron motion in the y direction). While the upper subband above this energy gap maintains a parabolic shape, the lower subband has a saddle point that results in a van Hove singularity in the density of states. With increasing $B_{\|}$, as the bottom of the upper subband moves above E_F, the density of states that contribute to scattering at the Fermi surface suddenly decreases, resulting in a minimum in R. As $B_{\|}$ is further increased, the top (saddle point) of the lower subband rises above E_F. Since the density of states at the saddle point diverges and electrons have zero group velocity, a resistance maximum is expected as the saddle point passes through E_F.

The resistance oscillation we observe in Fig. 2 can be understood based on a similar picture and considering that there are three dispersion parabolas in our TLES, as shown in the left panel of Fig. 3. The vertical positions of these parabolas are determined by the measured layer densities that depend on the applied V_{FG}, and their relative horizontal positions by the applied $B_{\|}$ and the distance between the adjacent layers (d) according to $\Delta k_y=edB_{\|}/\hbar$. To determine the layer densities, we did a Fourier transform analysis of the Shubnikov–de Haas oscillations at low $B_{\perp}$ and obtained the *subband* densities as a function of V_{FG}. The measured subband densities are shown in Fig. 4(b) together with the results of our self-consistent subband density calculations (solid curves), which are in excellent agreement with the experimental data. For the self-consistent calculations, we used 188 Å for the central well width and 154 Å for the width of the side wells, and 13 Å for the AlAs barrier width; these widths are very close to the growth parameters. Finally,

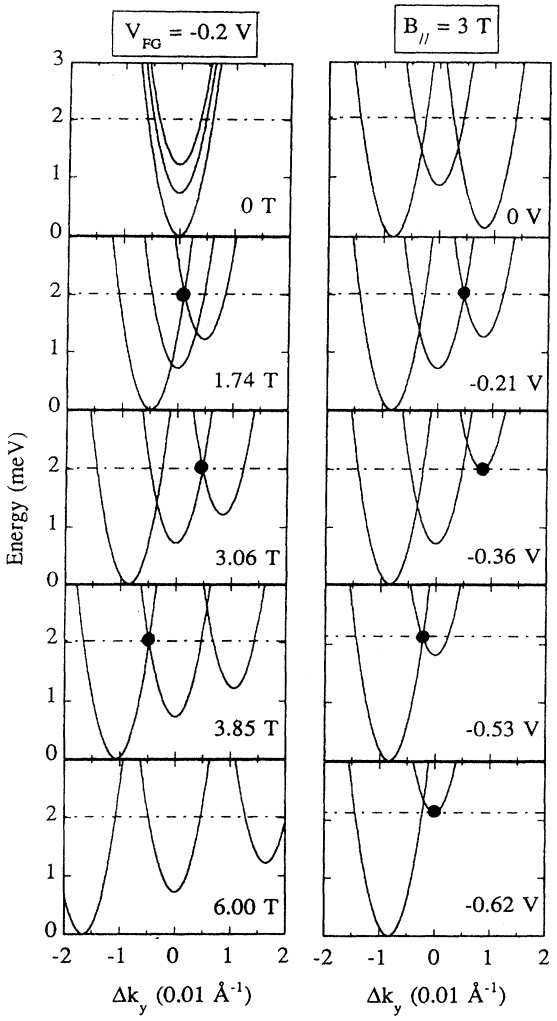

FIG. 3. Evolution of the dispersion parabolas for the TLES with $B_\parallel$ and V_{FG}. Left panel shows the evolution as a function of $B_\parallel$ at $V_{FG}=-0.2$ V. As $B_\parallel$ increases, the top-layer parabola shifts with positive Δk_y relative to the central-layer parabola and the bottom-layer parabola shifts with negative Δk_y. The right panel illustrates the case where a negative V_{FG} is applied at fixed $B_\parallel=3$ T. The Fermi level is indicated by the dash-dotted line. The solid circles denote layer depopulations or level anticrossings near which we expect resistance oscillations.

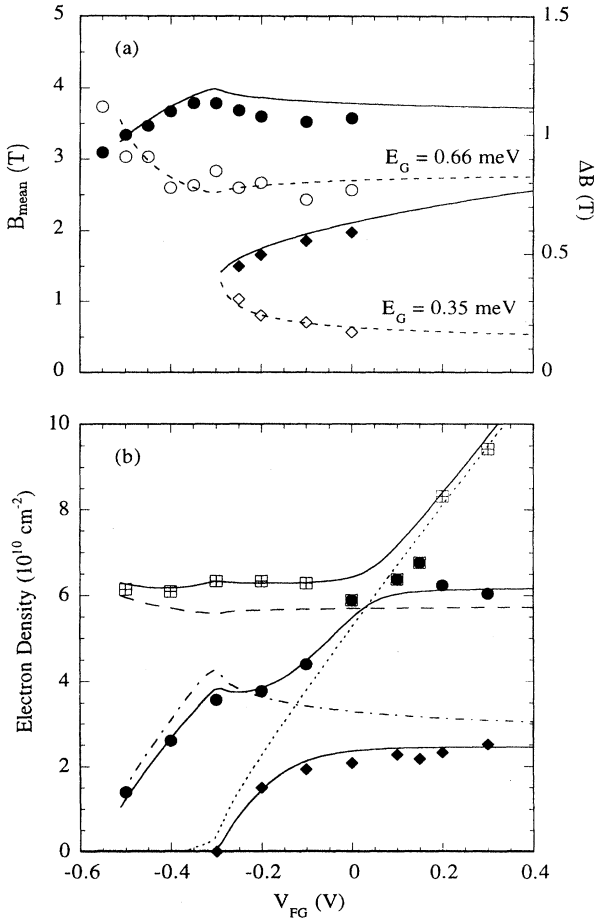

FIG. 4. (a) The solid circles and diamonds are the measured B_{mean} for central-bottom and top-bottom layer anticrossings and the solid curves are the calculated $B_\parallel$ for the anticrossings at different V_{FG}. The open circles and diamonds are the measured ΔB data, while the dashed curves are best fits to the data; for the fits, we used energy gaps equal to 0.66 meV for the central-bottom layer anticrossing and 0.35 meV for the top-bottom layer anticrossing. (b) The symbols show the subband densities measured from Shubnikov–de Haas oscillations and the solid curves are the subband densities from our self-consistent calculations. Also, the calculated top-, central-, and bottom-layer densities are shown by dotted, dashed-dotted, and dashed curves, respectively.

we deduced the *layer* densities by integrating under the charge distribution curve for each well. These densities that are also shown in Fig. 4(b) were used to determine the vertical positions of the parabolas with respect to E_F in Fig. 3. It is worth emphasizing that in our self-consistent calculation of the subband densities, we included the exchange term via a local-density approximation.[9] The inclusion of exchange is essential for a quantitative explanation of the measured subband densities and the positions of the R oscillations. In particular, the dominance of the exchange energy when the top layer is nearly depleted induces a significant charge transfer from the top layer to the central layer near $V_{FG}=-0.3$ V.[10] This charge transfer is responsible for the anomalous dependence of the position of R oscillation on V_{FG} as we will discuss later in the paper.

Let us now focus on the left panel of Fig. 3 that corresponds to the $V_{FG}=-0.20$ V experimental trace of Fig. 2. At $B_\parallel=0$ T, the three dispersion parabolas for the three layers are centered at $\Delta k_y=0$. As we gradually increase $B_\parallel$, the top- and bottom-layer parabolas shift horizontally by equal amounts but in opposite directions with respect to the central-layer parabola. At $B_\parallel=1.74$ T, the top and bottom parabolas intersect at E_F, and a partial energy gap results as these parabolas anticross.[11] This gap should be small because of the weak coupling between the top and bottom layers. As E_F passes through this small gap, we expect a weak R oscillation near $B_\parallel=1.74$ T; this is consistent with the experimental observation of a weak R oscillation near $B_\parallel=1.60$ T for $V_{FG}=-0.20$ V (Fig. 2). Similarly, the large R oscillations observed near $B_\parallel=2.8$ and 3.6 T can be related to E_F cross-

ing the energy gaps from the top-central anticrossing at $B_{\|}=3.06$ T and from the central-bottom anticrossing at $B_{\|}=3.85$ T, respectively. These oscillations have larger amplitudes consistent with the stronger coupling between the adjacent layers that results in larger anticrossing gaps.

Other traces of Fig. 2 data can also be explained through a similar analysis of the dispersion parabolas. At $V_{FG}=0$ V, we observe only two oscillations in Fig. 2. This is because the electron densities of the top and bottom layers are nearly equal at $V_{FG}=0$ V [Fig. 4(b)]. The dispersion parabolas of these two layers, therefore, intersect the central-layer parabola at the same $B_{\|}$ (≈ 3.6 T), resulting in only one strong R oscillation. Also, note that when V_{FG} is sufficiently negative (e.g., $V_{FG}=-0.40$ or -0.50 V) so that the top layer is completely depleted, only one R oscillation is observed, as expected for a bilayer system. Finally, for $V_{FG}=-0.65$ V, the system contains only one electron layer and the oscillation in R disappears.

From the data in Fig. 2, we plot in Fig. 4(a) the mean (B_{mean}) and difference (ΔB) of the $B_{\|}$ positions of the R maximum and minimum for the R oscillation arising from the top-bottom and central-bottom anticrossing gaps. While B_{mean} for the top-bottom anticrossing decreases monotonically with decreasing V_{FG} as the top layer is depleted, B_{mean} for the central-bottom anticrossing remains nearly constant, then *increases* with decreasing V_{FG} and reaches a maximum at $V_{FG}\approx -0.3$ V before finally decreasing at smaller V_{FG}. This anolamous behavior reflects the exchange-induced charge transfer from the top to the central layer as the top layer is depleted [Fig 4(b)]. For a quantitative comparison of the experimental B_{mean} and ΔB with the expected values, we used simple expressions given in Ref. 3 (Eqs. 3 and 4) and calculated B_{mean} and ΔB for the geometry and parameters of our sample.[12] The results are shown in Fig. 4(a) by solid and dashed curves and are in very good agreement with the experimental data. We note that there is no adjustable parameter in the calculation of B_{mean}, while for ΔB, the magnitude of the anticrossing energy gaps are used as fitting parameters. We used $E_G=0.35$ and 0.66 meV for the gaps arising from the anticrossings of the top-bottom and central-bottom layers, respectively. These gaps should be close to the *subband* energy splittings *in the absence of* $B_{\|}$ when the corresponding layers have equal densities and are in resonance.[3] From the data of Fig. 4(b), we deduce a subband splitting of 0.30 meV for the anticrossing of the top- and bottom-layer energy levels at $V_{FG}\approx 0.03$ V, and a splitting of 0.78 meV for the anticrossing of the central- and top-layer energy levels at $V_{FG}\approx -0.12$ V; these are consistent with the above E_G deduced from the measured ΔB.

Finally we turn to the R vs V_{FG} data in Fig. 1(b) where, in addition to the strong R oscillations at the layer transition V_{FG}, two other R oscillations (marked by arrows) are observed for intermediate $2.0<B_{\|}<3.5$ T. These two oscillations can be explained from the evolution of the dispersion parabolas with V_{FG} at fixed $B_{\|}$. As shown in the right panel of Fig. 3, at $B_{\|}=3$ T, for example, besides the layer depopulation R oscillations at $V_{FG}=-0.36$ and -0.62 V, we expect two other R oscillations near $V_{FG}=-0.21$ and -0.53 V as the anticrossing gaps of the top-central and central-bottom layers are swept above E_F, respectively. We attribute the R minima marked by arrows in Fig. 1(b) to the E_F passing through the upper level of these two anticrossing gaps. In agreement with this explanation, we observe these minima at progressively larger V_{FG} as $B_{\|}$ is increased from 2.0 to 3.5 T, in contrast to layer-depopulation R oscillations whose V_{FG} positions are independent of $B_{\|}$. We note, however, that the shape and position of these two oscillations are severely distorted because of the strongly increasing R background with decreasing V_{FG} and the R oscillations observed near the layer depopulation V_{FG}.

In summary, we observed resistance oscillations in a TLES as a function of front-gate bias and parallel magnetic field. The oscillations have two distinct origins: anticrossing of the layer dispersions in the presence of $B_{\|}$ and layer depopulation with decreasing front-gate bias. The data are quantitatively explained by the evolution of electron density in each layer and taking into account the effect of exchange-induced charge transfer.

We thank S. Parihar for help in self-consistent subband calculations and J. Jo and M. B. Santos in sample fabrication. This work was supported by the National Science Foundation and the Army Research Office.

[1] Y. W. Suen, L. W. Engel, M. B. Santos, M. Shayegan, and D. C. Tsui, Phys. Rev. Lett. **68**, 1379 (1992).

[2] J. P. Eisenstein, G. S. Boebinger, L. N. Pfeiffer, and S. He, Phys. Rev. Lett. **68**, 1383 (1992).

[3] J. A. Simmons, S. K. Lyo, N. E. Harff, and J. F. Klem, Phys. Rev. Lett. **73**, 2256 (1994).

[4] S. K. Lyo, Phys. Rev. B **50**, 4965 (1994).

[5] A. H. MacDonald, Surf. Sci. **229**, 1 (1990).

[6] J. Jo, Y. W. Suen, L. W. Engel, M. B. Santos, and M. Shayegan, Phys. Rev. B **46**, 9776 (1992).

[7] Y. Katayama, D. C. Tsui, H. C. Manoharan, and M. Shayegan, Surf. Sci. **305**, 405 (1994); Y. Katayama, D. C. Tsui, H. C. Manoharan, S. R. Parihar, and M. Shayegan (unpublished); X. Ying, S. R. Parihar, H. C. Manoharan, and M. Shayegan (unpublished).

[8] We note that our observation is different from the resistance maximum arising from the resonant interaction of electrons in a double-well system which has very different mobilities in each well. [A. Palevski, F. Beltram, F. Capasso, L. Pfeiffer, and W. West, Phys. Rev. Lett. **65**, 1929 (1990).]

[9] F. Stern and S. Das Sarma, Phys. Rev. B **30**, 840 (1984).

[10] A similar charge transfer is observed in bilayer electron systems. [J. P. Eisenstein, L. N. Pfeiffer, and K. W. West, Phys. Rev. B **50**, 1760 (1994); also see Ref. 7.]

[11] For clarity, the anticrossing gaps are not shown in Fig. 3. We address the size of these gaps later in the paper when we discuss the widths (in $B_{\|}$) of the R oscillations [Fig. 4(a)].

[12] For the calculation of B_{mean} and ΔB shown in Fig. 4(a), we used the layer densities self-consistently calculated at $B_{\|}=0$.